Self-Consistent Calculation of the Surface Photoelectric Effect*

Peter J. Feibelman
Sandia Laboratories, Albuquerque, New Mexico 87115
(Received 10 February 1975)

Surface photocurrents have been calculated using the same surface potential-barrier model to evaluate the initial and final photoelectron wave functions *and* the spatial behavior of the exciting electromagnetic field. The calculations show, for the jellium models employed, that total surface photoyield versus frequency is highly sensitive to surface electronic structure, while surface photocurrent energy and angle distributions are quite insensitive to it.

In this Letter, I report the first calculations of the surface photoelectric effect[1-4] in which the electromagnetic field responsible for photoemission has been calculated on the same microscopic footing as the initial and final photoelectron wave functions.[5] This self-consistent feature of the calculations makes it possible to ask what aspects of surface photoemission data should be sensitive to the electronic structure of a free-electron metal surface and which should not. As is shown below, the shapes of surface photoelectron energy and angular distributions appear to be relatively insensitive to surface structure, while the variation of total surface photoyield with frequency, ω, is highly sensitive to it.

Within the one-electron picture of the photoelectric effect,[6] for a flat, semi-infinite solid, the probability that an electron initially represented by the wave function[7] $\psi_i(z)\exp(i\vec{\rho}\cdot\vec{k}_\parallel)$ will be emitted in the final state corresponding to $\psi_f(z)\exp[i\vec{\rho}\cdot(\vec{k}_\parallel+\vec{q}_\parallel)]$ is governed by the (normalized) matrix elements $\mathfrak{M}_{fi}$ and $\mathfrak{M}_{fi}^{(c)}$ defined by

$$\{\mathfrak{M}_{fi},\mathfrak{M}_{fi}^{(c)}\}\equiv\int dz\{j_{fi}(z),j_{fi}^*(z)\}A_{\vec{q}_\parallel,\omega}^{z}(z)[A_{\vec{q}_\parallel,\omega}^{(T)z}(Z)]^{-1}, \tag{1}$$

where $j_{fi}(z)\equiv\psi_f^*(z)\,d\psi_i/dz-\psi_i(z)\,d\psi_f^*/dz$, and where $A^z(\vec{r},t)\equiv\mathrm{Re}\{A_{\vec{q}_\parallel,\omega}^{z}(z)\exp[i(\vec{q}_\parallel\cdot\vec{\rho}-\omega t)]\}$ is the z component of the vector potential[8] responsible for photoexcitation. The normalization factor $A_{\vec{q}_\parallel,\omega}^{(T)z}(Z)$ is the transverse part of $A_{\vec{q}_\parallel,\omega}^{z}(z)$ evaluated at a depth $z=Z$ sufficiently far inside the metal that $A_{\vec{q}_\parallel,\omega}^{(T)z}(z\gtrsim Z)$ can be assumed to be of its bulk form, $A_{\vec{q}_\parallel,\omega}^{(T)z}(Z)\exp[iq_\perp^{(T)}(z-Z)]$, where $q_\perp^{(T)}$ is the classical transmitted-wave wave vector.[9]

The important new aspect of the present calculation is that in evaluating $\mathfrak{M}_{fi}$ and $\mathfrak{M}_{fi}^{(c)}$, the same model of the surface was used not only to obtain $\psi_i(z)$ and $\psi_f(z)$, but also to obtain $A_{\vec{q}_\parallel,\omega}^{(z)}(z)$. Thus $\psi_i(z)$ and $\psi_f(z)$ were taken to satisfy the Schrödinger equation,[10]

$$\left[-\frac{\hbar^2}{2m}\frac{d^2}{dz^2}+V(z)-E_{i,f}^{(\perp)}\right]\psi_{i,f}(z)=0, \tag{2}$$

where $V(z)$ was a model one-electron surface potential barrier, e.g., a Lang-Kohn[11] self-consistent potential. At the same time, for a long-wavelength incident beam,[12] $A_{\vec{q}_\parallel\to 0,\omega}^{z}(z)$ was evaluated via the equation[5]

$$\mathfrak{A}_\omega(z)=\epsilon^T(\omega)-(4\pi i/\omega)\int dz'\,\sigma_\omega(z,z')\mathfrak{A}_\omega(z'), \tag{3}$$

wherein $\epsilon^T(\omega)$ is the bulk, long-wavelength, transverse dielectric constant, $\mathfrak{A}_\omega(z)\equiv A_{q_\parallel\to 0,\omega}^{z}(z)/A_{q_\parallel\to 0,\omega}^{(T)z}(Z)$, and $\sigma_\omega(z,z')$ is the z-z component of the metal's nonlocal conductivity tensor, evaluated as $|\vec{q}_\parallel|\to 0$. Both $\epsilon^T(\omega)$ and $\sigma_\omega(z,z')$ were calculated in the random-phase approximation which implies that $\epsilon^T(\omega)=1-\omega_p^2/\omega^2$ and that $\sigma_\omega(z,z')$ is given by

$$\sigma_\omega(z,z')=-\frac{e^2}{i\omega}\left\{\frac{n_0(z)}{m}\delta(z-z')+\frac{2}{\hbar}\int\frac{d^2k_\parallel}{(2\pi)^2}\int_{k,k'}\frac{\theta_{k_\parallel k'}-\theta_{k_\parallel k}}{\omega+i\delta-\omega_k+\omega_{k'}}\,j_{kk'}(z)j_{k'k}(z')\right\}. \tag{4}$$

In Eq. (4), the quantities $j_{kk'}(z)$, $n_0(z)$, and $\theta_{kk'}$, defined respectively by $j_{kk'}(z)\equiv(\hbar/2mi)[\psi_k^*(z)\,d\psi_{k'}/dz-\psi_{k'}(z)\,d\psi_k^*/dz]$, $n_0(z)\equiv(2\pi^3)^{-1}\int d^2k_\parallel\,dk\,\theta_{k_\parallel k}|\psi_k(z)|^2$, and $\theta_{k_\parallel k}\equiv\theta(\mathcal{E}_F-\hbar^2k_\parallel^2/2m-\hbar\omega_k)$ [$\theta(x)$ is the unit step function, $\mathcal{E}_F$ the Fermi energy], are all given in terms of the electron wave functions and en-

ergies $\psi_\kappa(z)$ and $\hbar\omega_\kappa$ which solve the Schrödinger equation,

$$\left(-\frac{\hbar^2}{2m}\frac{d^2}{dz^2}+V(z)-\hbar\omega_\kappa\right)\psi_\kappa(z)=0; \tag{5}$$

consequently the kernel $\sigma_\omega(z,z')$, and therefore also $\mathfrak{a}_\omega(z)$, are entirely specified by the choice of $V(z)$. Thus the results presented below are based on the numerical solution of Eqs. (2) and (3), followed by the evaluation of $\mathfrak{M}_{fi}$ and $\mathfrak{M}_{fi}^{(c)}$ via Eq. (1), and finally by the calculation of the differential quantum yield, $d^2Y/d\Omega_f\,dE_f$, of electrons emerging from the metal at angle $\Omega_f\equiv(\theta_f,\varphi_f)$ with energy E_f, per incident photon flux, according to the formulas[6]

$$d^2Y/d\Omega_f\,dE_f=(S/\cos\theta_I)\,|A_{\vec{q}_\parallel\to 0,\omega}^{(T)z}(Z)|^2\,|\vec{A}_{q_\parallel\to 0,\omega}^{(0)}|^{-2}\,Q_\omega(\Omega_f,E_f), \tag{6a}$$

$$Q_\omega(\Omega_f,E_f)\equiv(\alpha/\pi^2\hbar\omega)\,\theta(\hbar\omega-\Phi-E_f)\,\theta(E_f^{(\perp)}+\Phi+\mathcal{E}_F-\hbar\omega)$$
$$\times[E_f/(E_f^{(\perp)}+\Phi+\mathcal{E}_F-\hbar\omega)]^{1/2}[|\mathfrak{M}_{fi}|^2+|\mathfrak{M}_{fi}^{(c)}|^2]_{E_i^{(\perp)}=E_f^{(\perp)}-\hbar\omega}. \tag{6b}$$

In Eqs. (6), S is the sample surface area, θ_I is the angle of photon incidence, $\vec{A}_{q_\parallel\to 0,\omega}^{(0)}$ is the incident beam amplitude,[13] α is the fine-structure constant, and Φ is the metal's work function. Finally note that $E_f^{(\perp)}\equiv E_f\cos^2\theta_f$.

In Fig. 1, typical results are shown for $\mathfrak{a}_\omega(z)$, in this case for $V(z)$ chosen to equal the Lang-Kohn potential barrier[11] corresponding to electron gas radius $r_s=2$. Note that for ω well below ω_p, the classical plasma frequency [$\hbar\omega_p(r_s=2)=16.7$ eV], both the magnitude and the phase of $\mathfrak{a}_\omega(z)$ vary rapidly in the surface region [i.e., in the neighborhood of $z=0$],[14] and moreover that the behavior of $\mathfrak{a}_\omega(z)$ is strongly ω dependent. Near to and above ω_p, the strong surface peak in $|\mathfrak{a}_\omega(z)|$ disappears, and above ω_p, the Friedel-like decaying oscillations of $\mathfrak{a}_\omega(z)$ inside the metal are replaced by nondecaying, sinusoidal (bulk plasmon) oscillations.[15] Thus, correlating the strength of the surface photoyield with $|\mathfrak{a}_\omega(z\approx 0)|^2$, one would expect it to be large and strongly frequency dependent below ω_p and to be much weaker above ω_p.

These expectations are borne out in Fig. 2, which shows $Q_\omega\equiv\int d\Omega_f\,dE_f\,Q_\omega(\Omega_f,E_f)$ as a function of ω, not only for the $r_s=2$ Lang-Kohn potential, but also for a variety of other potential barriers and values of r_s. The curves labeled $r_s=2$, 3, and 4 in Fig. 2 were calculated using the Lang-Kohn potential barriers for those values of r_s. Note that in each case Q_ω is much larger for $\omega<\omega_p$ than for $\omega>\omega_p$, and also that Q_ω varies considerably with ω. The curves labeled $a=0.33$, 0.66, and 0.99 Å in Fig. 2 were calculated for r_s

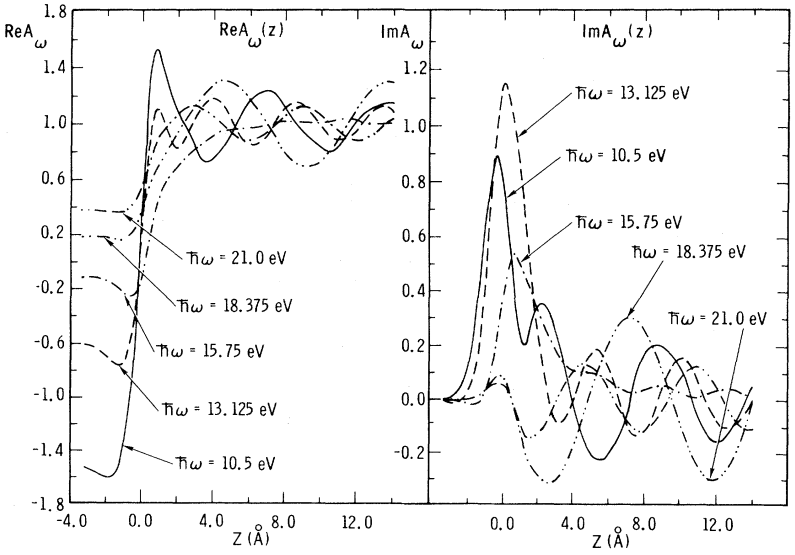

FIG. 1. Real and imaginary parts of $\mathfrak{a}_\omega(z)$ for various frequencies, ω, calculated using the $r_s=2$, Lang-Kohn potential barrier (Ref. 11).

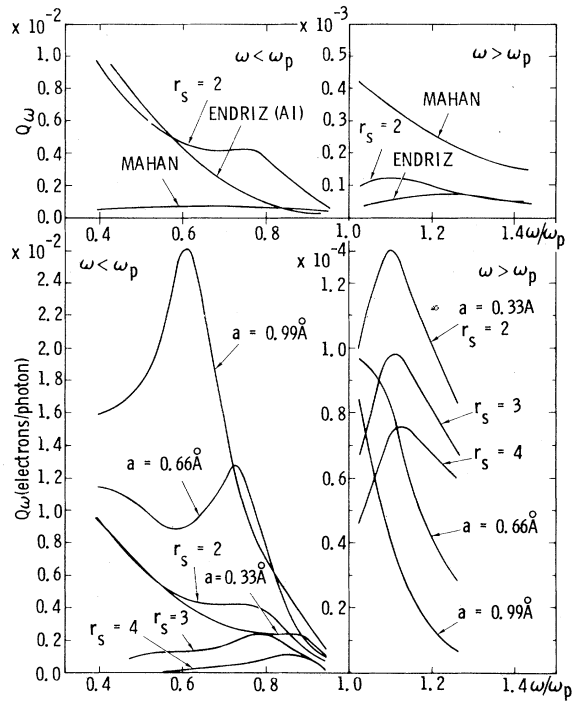

FIG. 2. Total quantum yield Q_ω versus frequency for a variety of models of surface electronic structure (identified in the text).

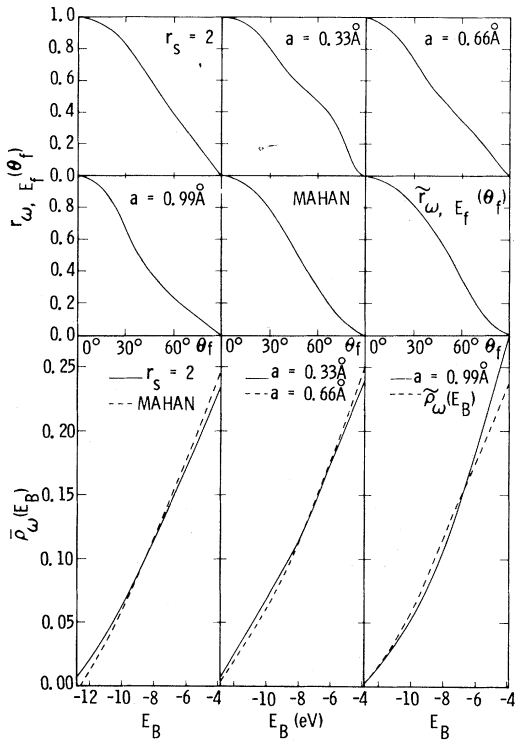

FIG. 3. Surface photoelectron angle distributions $r_{\omega, E_f=5.44\ \mathrm{eV}}(\theta_f)$, and energy distributions $\bar{\rho}_\omega(E_s) \equiv \rho_\omega(E_f - \hbar\omega)$, for $\hbar\omega = 13.25$ eV, and for various $r_s = 2$ surface barrier models (identified in the text). Also shown for comparison are the functions

$$\tilde{r}_{\omega, E_f}(\theta_f) \equiv \cos^2\theta_f \left(\frac{E_f + \Phi + \mathcal{E}_F - \hbar\omega}{E_f \cos^2\theta_f + \Phi + \mathcal{E}_F - \hbar\omega} \right)^{1/2},$$

with $E_f = 5.44$ eV and $\hbar\omega = 13.125$ eV, and

$$\tilde{\rho}_\omega(E_B) \equiv \int d\theta_f\, \bar{r}_{\omega, E_B + \hbar\omega}(\theta_f) / \int d\theta\, dE\, \bar{r}_{E+\hbar\omega}(\theta),$$

for $\hbar\omega = 13.125$ eV. (For all curves, I used $\Phi = 3.89$ eV and $\mathcal{E}_F = 12.6$ eV.)

$= 2$, using the potential[16]

$$V_a(z) = -\frac{[\Phi(r_s = 2) + \mathcal{E}_F(r_s = 2)]}{1 + \exp\{-[z/a + (z/5a)^3]\}}. \qquad (7)$$

Thus the comparison of these curves among themselves and with those labeled $r_s = 2$ reveals the strong sensitivity of the total photoyield to surface electronic structure. For example the strength of the surface photoeffect is 6 times greater, for $\omega/\omega_p \approx 0.6$, using the rather diffuse potential with $a = 0.99$ Å than using the self-consistent Lang-Kohn barrier. Not only the magnitude but also the shapes of the Q_ω versus ω curves seem to be surface-structure dependent. Thus in each of the curves corresponding to $r_s = 2$ there is a peak in Q_ω for $\omega < \omega_p$; but the peak moves closer to ω_p and decreases in magnitude as the potential barrier is taken to be less diffuse.

In view of the strong sensitivity of Q_ω to surface structure exhibited in the lower panels of Fig. 2, the results shown in the upper ones are perhaps not too surprising. In these panels Q_ω for the $r_s = 2$ Lang-Kohn potential is compared to Q_ω calculated for a square-step potential and assuming $\mathfrak{A}_\omega(z)$ to be everywhere equal to 1 (curves labeled "Mahan"[2]), and to Q_ω calculated using a square-step plus image-force potential and using a form of $\mathfrak{A}_\omega(z)$ calculated hydrodynamically, representing the metal's conductivity by its bulk value [curves labeled "Endriz (Al)"[1]]. Again one notes that the results are markedly different for the different surface models, and particularly that the neglect of refraction effects (Mahan curves) results in a Q_ω which is far too small for $\omega < \omega_p$ and too large for $\omega > \omega_p$.

The strong sensitivity of Q_ω to surface electronic structure does not carry over to the shapes of the normalized surface photoelectron energy and angular distributions, $\rho_\omega(E_f) \equiv \int d\Omega_f\, Q_\omega(\Omega_f, E_f)/Q_\omega$ and $r_{\omega, E_f}(\theta_f) \equiv Q_\omega(\theta_f, \varphi_f, E_f)/Q_\omega(0, \varphi_f, E_f)$, a fact illustrated in Fig. 3. Indeed one can fit these curves simply by taking account of the fact that

if $V(z)$ has no eigenstate at the vacuum level then $\psi_f(z)$ must vanish linearly in $\sqrt{E_f^{(\perp)}}$ as $E_f^{(\perp)} \to 0$. Thus, assuming that $|\mathfrak{M}_{f_i}|^2 + |\mathfrak{M}_{f_i}^{(c)}|^2$ behaves as a constant times $E_f^{(\perp)}$, one has from Eq. (6b) that $r_{\omega, E_f}(\theta_f)$ should be proportional to $\cos^2\theta_f / [E_f \cos^2\theta_f + \Phi + \mathcal{E}_F - \hbar\omega]^{1/2}$, and $\rho_\omega(E_f)$ to $E_f^{3/2}$ times the θ_f integral of this function. Both of these estimates seem roughly correct.

Two important aspects of surface photoemission remain to be treated[17]: the effects of roughness and of a finite relaxation time, τ. Although a limited set of photoyield (versus incidence angle) data has been published[18] which appears to represent surface photoemission from smooth Al films, most available photoemission data from free-electron metals seem to be strongly influenced by surface roughness. That is, the fact that photoelectron energy distributions from free-electron metal films seem (particularly at lower values of ω)[19] to be quite generally sawtooth-shaped[20] even though the incident beam is normal to the surface is strongly suggestive of the idea that these photoelectron energy distributions are in fact the result of roughness-induced surface photoemission.[21] Thus to compare theory and experiment for free-electron metals it would be useful to have more data from smooth samples as well as theoretical results for rough ones. It would also be useful to learn what effects result from the introduction of a finite τ into the theory—in particular one wants to know the extent to which τ might decrease the surface-structure sensitivity of Q_ω in the lower-frequency range, $\omega/\omega_p \approx 0.4 - 0.8$.

---

*Work supported by the U. S. Energy Research and Development Administration.

[1]J. G. Endriz, Phys. Rev. B 7, 3464 (1973). Here the spatial behavior of the electromagnetic field was calculated using an essentially *ad hoc* prescription: Electron-gas dielectric response was treated hydrodynamically in bulk and this hydrodynamic behavior was interpolated through the surface region via a convolution with the unperturbed electron-density profile.

[2]G. D. Mahan, Phys. Rev. B 2, 4334 (1970).

[3]W. L. Schaich and N. W. Ashcroft, Phys. Rev. B 3, 2452 (1971).

[4]I. Adawi, Phys. Rev. 134, A788 (1964). This paper includes a list of earlier references concerning the surface photoeffect.

[5]For details of the field calculation, see P. J. Feibelman, to be published.

[6]See, e.g., P. J. Feibelman and D. E. Eastman, Phys. Rev. B 10, 4932 (1974).

[7]The surface is taken to lie in an x-y plane, with the metal in the right half-space. The vector $\vec{\rho} \equiv (x,y)$.

[8]I use the gauge in which the scalar potential is identically zero.

[9]$q_\perp^{(T)2} = [\epsilon^T(q^{(T)},\omega) - \sin^2\theta_I]\,\omega^2/c^2$, where $\epsilon^T(q^{(T)},\omega)$ is the metal's transverse dielectric constant, θ_I is the angle of incidence, c is the speed of light, and $q^{(T)2} = q_\perp^{(T)2} + |\vec{q}_\parallel|^2$.

[10]Together with appropriate boundary conditions; see Ref. 6. Note that in the present calculations the final-electron mean free path, $\lambda(E_f)$, has been taken to be infinite. This approximation is valid in the energy range considered ($\omega/\omega_p \lesssim 1.4$) because $\lambda(E_f \lesssim 1.4\hbar\omega_p - \Phi)$ is typically >15 Å while surface photoexcitation occurs mainly within a few angstroms of the surface.

[11]N. D. Lang and W. Kohn, Phys. Rev. B 1, 4555 (1970).

[12]And also assuming that $|q_\perp{}^T|$ (cf. Ref. 9) is small.

[13]The incident flux of photons per unit area per unit time equals $(\omega^2|\vec{A}_{\vec{q}_\parallel \to 0,\omega}^{(0)}|^2/8\pi c)/\hbar\omega$.

[14]The positive background charge of the jellium metal is assumed to be of the form $-n_\infty\theta(z)$.

[15]Cf. A. R. Melnyk and M. J. Harrison, Phys. Rev. B 2, 835 (1970); K. L. Kliewer, Phys. Rev. Lett. 33, 900 (1974).

[16]The value of $\Phi(r_s = 2)$ was taken from Ref. 11.

[17]Of course for comparison with real metals, *bulk* photoemission [caused by the presence of a periodic crystal potential] should also be taken into account.

[18]S. A. Flodström and J. E. Endriz, Phys. Rev. Lett. 31, 893 (1973).

[19]Where secondaries are unimportant.

[20]See Ref. 1 and references listed therein.

[21]Specifically (cf. Ref. 1) via the intermediate step of surface-plasmon generation.